RESEARCH ARTICLE

Key Point:
- Seasonal mixed layer depth adjustment in eddies could modulate chlorophyll

Correspondence to:
F. Dufois,
francois.dufois@csiro.au

Impact of eddies on surface chlorophyll in the South Indian Ocean

François Dufois[1], Nick J. Hardman-Mountford[1], Jim Greenwood[1], Anthony J. Richardson[2,3], Ming Feng[1], Steven Herbette[4,5], and Richard Matear[6]

[1]CSIRO Oceans and Atmosphere Flagship, Wembley, Western Australia, Australia, [2]CSIRO Oceans and Atmosphere Flagship, Ecosciences Precinct, Brisbane, Queensland, Australia, [3]Centre for Applications in Natural Resource Mathematics, School of Mathematics and Physics, University of Queensland, St. Lucia, Queensland, Australia, [4]LMI ICEMASA, Department of Oceanography, University of Cape Town, Cape Town, South Africa, [5]Laboratoire de Physique des Océans, (UMR6523 CNRS IFREMER IRD UBO), Université de Bretagne Occidentale, Brest, France, [6]CSIRO Oceans and Atmosphere Flagship, Hobart, Tasmania, Australia

Abstract A unique feature of the subtropical South Indian Ocean is the existence of anticyclonic eddies that have higher chlorophyll concentrations than cyclonic eddies. Off Western Australia, this anomalous behavior is related to the seeding of anticyclonic eddies with shelf water enriched in phytoplankton biomass and nutrients. Further off-shore, two mechanisms have been suggested to explain the eddy/chlorophyll relationship: (i) eddies originating from the Australian coast maintain their chlorophyll anomaly while propagating westward; and (ii) eddy-induced Ekman upwelling (downwelling) enhances (dampens) nutrient supply in anticyclonic (cyclonic) eddies. Here we describe the relationship between eddies and surface chlorophyll within the South Indian Ocean, and discuss possible mechanisms to explain the anomalous behavior in light of new analyses performed using satellite chlorophyll data. We show that anticyclonic eddies exhibit higher surface chlorophyll concentration than cyclonic eddies across the entire South Indian Ocean basin (from 20 to 28°S), particularly in winter. Using Self Organizing Maps we analyze the chlorophyll patterns within anticyclonic eddies and cyclonic eddies and highlight their complexity. Our analysis suggests that multiple mechanisms may underlie the observed eddy/chlorophyll relationship. Based on Argo float data, we postulate the relationship may be partly related to seasonal adjustment of the mixed layer depth within eddies. Deeper mixing in anticyclonic eddies is expected to enhance nutrient supply to the mixed layer, while shallower mixing in cyclonic eddies is expected to reduce it. This could explain why the observed winter surface chlorophyll bloom is stronger in anticyclonic eddies than in cyclonic eddies.

1. Introduction

Mesoscale eddies are common features of the oceanic circulation [*Chelton et al.*, 2011b], and play an important role in boosting biological production [e.g., *Klein and Lapeyre*, 2009; *McGillicuddy et al.*, 1998]. In the interior of eddies, the "eddy-pumping" paradigm relates vertical velocities to the change of density anomalies during eddy formation or intensification [*Klein and Lapeyre*, 2009; *McGillicuddy et al.*, 1998]. Following this concept, the conventional view in the open ocean is that cyclonic eddies (CEs) upwell nutrient-rich subsurface water into the euphotic zone, and are relatively productive, while anticyclonic eddies (ACEs) deepen the nutricline, and are relatively unproductive [*McGillicuddy and Robinson*, 1997; *McGillicuddy et al.*, 1998; *Oschlies and Garcon*, 1998]. However, in some regions the "eddy-pumping" concept does not explain the surface chlorophyll *a* (CHL) signature within eddies, suggesting other processes may dominate [*José et al.*, 2013; *McGillicuddy et al.*, 2007; *Quartly and Srokosz*, 2003].

Eddy-induced Ekman pumping, due to the interaction between eddy surface currents and winds, generates upwelling in the interior of ACEs, and downwelling in the interior of CEs [*Gaube et al.*, 2013]. This eddy-induced Ekman pumping has been suggested as a mechanism to explain enhanced nutrient supply to the surface within ACEs in the North Atlantic [*Martin and Richards*, 2001; *McGillicuddy et al.*, 2007] and the Southwest Indian Ocean [*Gaube et al.*, 2013].

Other processes can create differences in surface CHL between ACEs and CEs. For example, in the Mozambique Channel, horizontal entrainment of nutrient-rich coastal waters can cause ACEs to have higher CHL at their centre [*José et al.*, 2013]. Elsewhere, large submesoscale vertical velocities [*Lapeyre and Klein*, 2006;

Lévy et al., 2001; *Mahadevan et al.*, 2008] have been suggested to increase nutrient supply and primary production in ACEs [*Lévy and Klein*, 2004; *Mahadevan et al.*, 2008].

The eastern part of the South Indian Ocean is another region where the "eddy-pumping" concept does not explain the pattern of CHL in eddies. ACEs in this region generally contain higher phytoplankton concentrations than CEs, especially during the austral winter [*Dietze et al.*, 2009; *Gaube et al.*, 2013; *Pearce and Griffiths*, 1991; *Waite et al.*, 2007]. Off Western Australia, this phenomenon has been related to the seeding of ACEs with shelf water containing elevated nutrient and phytoplankton biomass [*Dietze et al.*, 2009; *Feng et al.*, 2007; *Greenwood et al.*, 2007]. Offshore of Western Australia, *Brewin et al.* [2012] highlighted a positive correlation between sea surface height (SSH) and CHL, across a large part of the basin, and suggested that it might be explained by the westward propagation of Leeuwin Current ACEs. It has also been suggested that the higher initial CHL concentration within ACEs could be supplemented by submesoscale injection of nutrients along the eddy edges [*Moore et al.*, 2007]. More recently, based on satellite CHL, SSH and wind data, *Gaube et al.* [2013] proposed eddy-induced Ekman pumping (reaching ± 10 cm d^{-1}) as a mechanism at least partly responsible for sustaining positive phytoplankton anomalies in ACEs in the South Indian Ocean.

The main proposed explanations for the anomalous character of South Indian Ocean eddies are problematic for several reasons. The ACEs that form from productive shelf water propagate slowly westward, and to maintain an elevated signature in these eddies across the basin would require retention of the nutrients within these eddies for many years, which seems unlikely [*Dietze et al.*, 2009; *Greenwood et al.*, 2007]. Meanwhile, the impact of eddy-induced Ekman pumping in the South Indian Ocean is yet to be properly demonstrated. Here we further investigate the link between eddies and surface CHL in the South Indian Ocean. We explore whether the unusual relationship between eddies and CHL is due to: (i) eddy-induced Ekman pumping; or (ii) westward propagation of productive shelf water. We start by describing the spatial and temporal variability of satellite CHL within South Indian Ocean eddies. We then use Self Organizing Maps (SOM) analysis to identify the main patterns of surface CHL within both ACEs and CEs. Finally we use data from Argo floats to compare vertical fluxes of nutrient into the mixed layer induced by either eddy-induced Ekman pumping or seasonal Mixed Layer Depth (MLD) change.

2. Material and Methods

2.1. Data

Our analysis is based on 9 km SeaWiFS satellite observations of oceanic CHL at weekly resolution from September 1997 to December 2010. To fill gaps in the CHL data set due to cloud cover, we applied a temporal low-pass filter, removing variability shorter than a month. CHL data were also smoothed using a spatial $1° \times 1°$ low-pass filter. This product is referred to as CHL. To remove the potential impact of larger structures such as Rossby waves, the CHL was high-pass filtered spatially to attenuate zonal scales >8° of longitude. This product is referred to as $\tilde{CHL}$.

We also used the eddy database from *Chelton et al.* [2011b] from October 1992 to January 2011. In this database eddy radius averaged ~100 km over the South Indian Ocean. For each eddy over the SeaWiFS period, we colocated the CHL field. Distances from eddy centres r were normalized by the eddy radius R (i.e., location of strongest geostrophic current), and the associated CHL field was projected into the normalized "eddy frame" (i.e., for each individual eddy, CHL values at distance r are projected to r/R). This allowed us to present statistics on eddy parameters (e.g., median) within eddy centroids ($r/R \leq 1$) and outer-perimeter eddy water ($r/R \geq 1$). Differences between CHL in ACEs and in CEs were tested using a Student's t test with significant differences defined as $p < 0.05$. Since CHL values have been described to follow a log-normal distribution [*Campbell*, 1995], the Student's t test was performed over the $\log_{10}$ transformed CHL.

Normalized CHL anomalies (hereafter called CHL') were also used for each individual eddy and were computed as:

$$CHL' = \frac{CHL - \overline{CHL}}{\sigma\left(CHL - \overline{CHL}\right)} \tag{1}$$

where $\overline{CHL} = \frac{1}{4\pi R^2} \int_0^{2\pi} \int_0^{2R} CHL \; r \; dr \; d\theta$ is the mean CHL and σ is the standard deviation, both computed over the eddy for $r \leq 2R$.
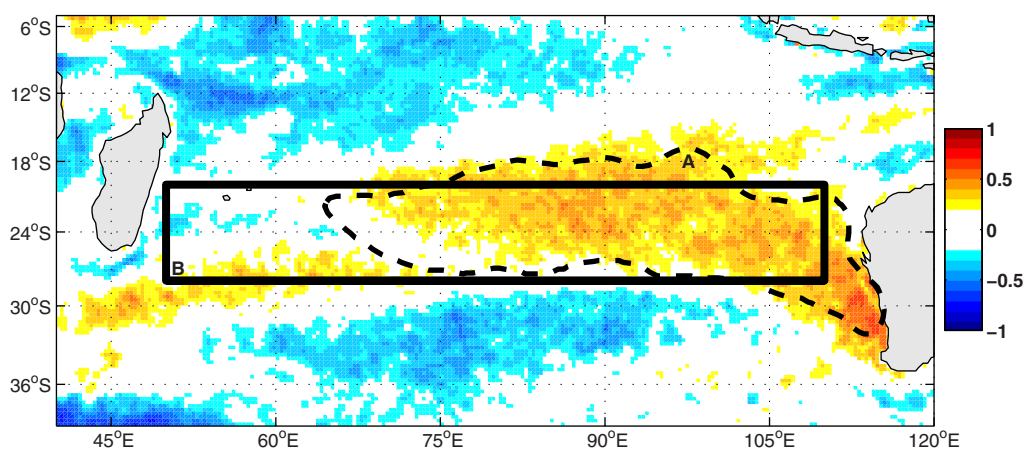
Figure 1. The correlation between S$\tilde{S}$H and C$\tilde{H}$L. The dotted contour is denoted as Region A and the black box is referred to as Region B.

We used all temperature and salinity profiles from Argo floats (downloaded from http://www.argo.net) that coincided with the eddy database period. Argo floats were first collocated with eddies. Climatologies of temperature and salinity profiles were then computed from floats within ACEs and CEs for $r/R \leq 1$ and from all floats in the region of interest. The MLD was computed from the Argo temperature profiles following *de Boyer Montégut et al.* [2004], where the base of the mixed layer corresponds to the depth where temperature changes by 0.2°C compared to the temperature at 10 m depth. We also computed the squared buoyancy (Brunt-Väisälä) frequency N^2 using $N^2 = -g/\rho_0 \frac{\partial \rho}{\partial z}$ with ρ the potential density calculated from temperature and salinity, g the gravitational acceleration, and the reference density $\rho_0 = 1025$ kg m^{-3}. N^2 is commonly used to assess water column stratification (e.g., the buoyancy production term of turbulent kinetic energy in vertical turbulent closure models relies on N^2) [*Warner et al.*, 2005].

This study used the weekly absolute dynamic topography provided on a 1/3° × 1/3° grid by AVISO (http://www.aviso.oceanobs.com/) over the SeaWiFS period (September 1997 to December 2010). This is referred to as SSH. The SSH was high-pass filtered to attenuate zonal scales >8° of longitude. This filtered product is referred to as S$\tilde{S}$H.

2.2. SOM Analysis

We used Self Organizing Maps [*Kohonen*, 2001], a type of artificial neural network, to identify the main surface CHL' patterns within eddies. We implemented the SOM in the MATLAB® SOM Toolbox 2.0. SOM is a powerful technique to identify representative patterns in large and complex data sets. It projects high-dimensional input data into a low dimensional (two-dimensions here) space and arranges the results topologically. Underlying patterns can therefore be visualized in the same form as the original data; here the patterns show maps of CHL' in the core of a "normalized" eddy. An analysis of the optimal number of patterns, from 9 to 100, suggested that 25 patterns, arranged in a 5x5 array, were sufficient to represent the variability in our CHL' data. This array is "self-organized," with more similar patterns in closer proximity, and more dissimilar patterns further apart. The four corners of the SOM represent the most extreme patterns, with a smooth continuum in between. The fraction (in %) of eddies that best resemble each SOM pattern is also given. These values depend on the initial number of patterns chosen for the analysis, and cannot be interpreted in terms of explained variance.

To assess the fraction of the variability in CHL' pattern within eddies that is captured by the SOM analysis, we computed the spatial correlation coefficient (Cor) between each individual eddy CHL' field and the best matching SOM pattern (for each eddy we picked up one different SOM pattern). Three proxies were then derived: (i) the 10th percentile of Cor; (ii) the median of Cor; and (iii) the fraction of eddies having one of the SOM patterns explaining >50% of their spatial variability (i.e., Cor>0.71). The same proxies were also used to assess the variability of the CHL' pattern explained by the median CHL' patterns.

Gaube et al. [2013] presented the median eddy patterns of chlorophyll anomaly over a region where the correlation between eddy-induced Ekman pumping velocity and chlorophyll anomaly exceeded 0.2 (Region

A on Figure 1). The SOM analysis was performed over the same Region A for the whole set of eddies (2949 CHL' images within ACEs and 2498 CHL' images within CEs), so that the SOM patterns were directly comparable with the median eddy patterns presented by *Gaube et al.* [2013].

2.3. Mixed Layer Nitrate Budget

To compare the different vertical fluxes of nitrate to the mixed layer, we used a nitrate budget equation derived from the formulation proposed by *Caniaux and Planton* [1998] for the mixed layer heat budget. The rate of change of nitrate within the mixed layer is:

$$\frac{\partial \bar{C}}{\partial t} = -\frac{1}{h}\left\{(\bar{C} - C_{-h})\left[\frac{\partial h}{\partial t} + w_{-h}\right]\right\} + residual \qquad (2)$$

where h is the MLD, C is the nitrate concentration, and w is the vertical velocity. C_{-h} and w_{-h} are the nitrate concentration and the vertical velocity at the base of the mixed layer. $\bar{C}$ is the vertical average of C over the mixed layer (i.e., $\bar{C} = \frac{1}{h}\int_{-h}^{0} C dz$). The term $\frac{\partial h}{\partial t} + w_{-h}$ corresponds to the entrainment rate (in m s^{-1}).

In this study, the budget was calculated from the surface to 2 m below the MLD. We focused on comparing two components of the entrainment rate in ACEs and CEs: the seasonal change of MLD and the eddy-induced Ekman pumping. Therefore, the *residual* term, which includes the flux of nitrate due to vertical turbulent mixing at the base of the mixed layer and horizontal divergence terms, was not considered. Following *Wong et al.* [1998], the change of MLD was set to 0 in Equation 2 when the mixed layer was shoaling ($\frac{\partial h}{\partial t} < 0$), so that only a deepening of the mixed layer could alter the concentration $\bar{C}$. In this study, eddy-induced Ekman pumping velocities were not computed from wind data. Instead, we used the velocities reported by *Gaube et al.* [2013] for eddies spawned from the Leeuwin Current (w_{-h}=7.8 cm d^{-1} in ACEs and w_{-h} =−5.9 cm d^{-1} in CEs). Eddy-induced Ekman pumping in the vicinity of the Leeuwin Current and in the rest of the South Indian Ocean have been shown to be quite similar [*Gaube et al.*, 2013].

The seasonal change of MLD ($\frac{\partial h}{\partial t}$) was computed from the climatological median of MLD derived from Argo floats over Region B (cf. Figure 1), using 1473 Argo profiles in ACEs and 1421 Argo profiles in CEs. Region B was chosen as a rectangular section of the South Indian Ocean where, on average, ACEs present higher CHL values than CEs.

We also compared the fluxes of nitrate into the mixed layer due to the seasonal change of MLD and the eddy-induced Ekman pumping in both ACEs and CEs. The impact of the nitrate concentration (i.e., $\bar{C} - C_{-h}$) on the flux was, however, difficult to estimate. Indeed, ARGO floats do not measure the nitrate concentration and the database of nitrate concentration in the South Indian Ocean was too small to differentiate between ACEs and CEs. As a first approximation, we used the nitrate seasonal climatology from the World Ocean Atlas 2009 [*Garcia et al.*, 2010] over Region B to estimate fluxes. Note that the existence of eddies will also modify the vertical profile of nitrate, however, this effect is not considered in our calculation.

To compare nitrate fluxes with the CHL rate of change, we converted the CHL values (in mg m^{-3}) into phytoplankton nitrogen biomass (in mmol m^{-3}). Because the South Indian Ocean is dominated by picophytoplankton [*Not et al.*, 2008], we used carbon-to-chlorophyll ratios in the range 65–176, corresponding to prymnesiophytes, green algae, prochlorococcus and other cyanobacteria [*Sathyendranath et al.*, 2009]. The Redfield ratio [*Redfield*, 1958] was then used to derive potential phytoplankton nitrogen biomass from carbon biomass.

3. Results

3.1. Eddy and CHL Relationship

There are significant positive correlations between SS̃H and CH̃L west of Western Australia (Figure 1). The relationship between SSH and CHL at the mesoscale in the South Indian Ocean averages r=0.27 (p=0.014) over Region A. The monthly relationship between eddies and CHL across the South Indian Ocean (inside Region B) are reported in Figure 2. Surface CHL concentrations within CE and ACE interiors ($r/R \leq 1$) are rather low (∼0.1 mg m^{-3}), with higher values along the coast on both sides of the basin and a net decrease toward the centre. A clear seasonal cycle is apparent, with an overall increase in the surface CHL during austral winter, peaking around July. The seasonality of the CHL within eddies is in phase across the basin.

Moreover, there is a link between the CHL seasonality and the CHL response within eddies. During winter, the CHL distribution is generally significantly higher within ACEs than CEs (p=0.0019 on average over
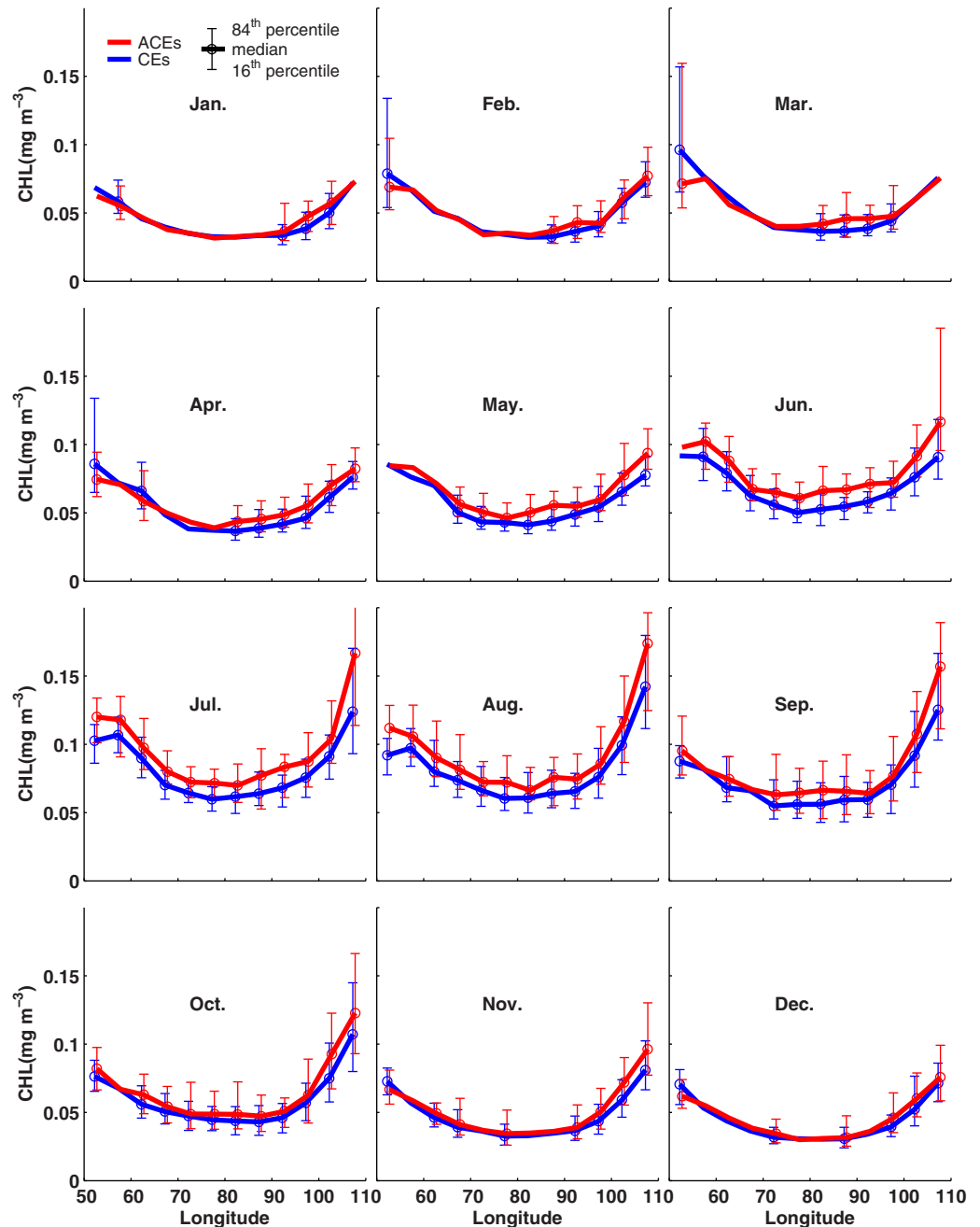
Figure 2. Longitudinal profiles of CHL over CE (blue) and ACE (red) interiors (r/R≤1) for each month and from 20°S to 28°S. The lines represent the median CHL values. If ACE and CE CHL distributions are significantly different (p<0.05), data distribution parameters are added: median values, represented by circles, are surrounded by the 16th and 84th percentiles (i.e., mean ±1 standard deviation for normal distribution), represented by vertical bars.

Region B during June/July/August) across the entire basin (Figure 2). Longitudinal profiles of monthly median CHL outside eddy interiors coherently fit between profiles of median CHL for ACEs and CEs (not shown), hence ACEs exhibit a positive anomaly and CEs exhibit a negative anomaly compared with the median CHL. This is observed across the whole basin from June to August and west of 80°E from April to October. On average over June/July/August inside Region B, the difference between ACEs and CEs reaches 14.4% of the median CHL value. There are however some overlaps between the two distributions at the extremes; some CEs can have higher CHL values than some ACEs. Moreover, there is no evidence of westward propagation of the CHL anomaly by eddies. Indeed, the difference between ACEs and CEs peaks in
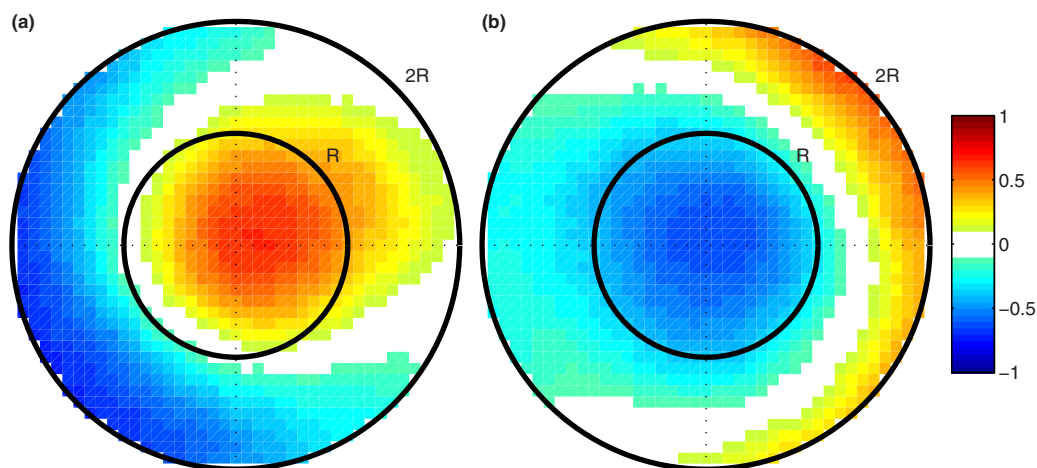
Figure 3. Median CHL' patterns in winter (June/July/August) in Region A within (a) ACEs and (b) CEs. Inner and outer circles respectively coincide with r/R=1 and r/R=2.

winter throughout the entire basin with no obvious time lag in the maximum CHL anomaly, between ACEs and CEs in the Leeuwin Current region (∼110°E) and the rest of the basin.

During summer, the difference between CHL in CEs and ACEs is lowest and less significant (p=0.26 on average over Region B during December/January/February). West of 70°E, eddies exhibit an opposite behavior from January to April, with CEs having overall higher surface CHL values.

3.2. Surface CHL Patterns Within Eddies in Winter

The spatial patterns of normalized CHL anomaly (CHL') observed during winter (June/July/August) provide more detail on the CHL difference between CEs and ACEs. The median patterns of CHL' show that higher values of CHL within ACEs during winter coincide with a positive anomaly of CHL centred in the middle of the eddy (Figure 3a). Conversely, lower values of CHL within CEs during winter coincide with a negative anomaly of CHL centred in the middle of the eddy (Figure 3b).

Median patterns can hide the underlying variability in CHL. Indeed, the median of the spatial correlation between each individual eddy CHL' pattern and the median pattern are 0.38 for ACEs and 0.33 for CEs during winter (Table 1). In winter, median patterns can only explain more than 50% of the spatial variability in 7.3% of the ACEs and 5.4% of the CEs. Although we focus on winter patterns, the median CHL' pattern is a poor representation of the variability for any season (cf. summer in Table 1).

Table 1. Spatial variability of CHL' in ACEs and CEs explained by the median patterns and the best matching SOM pattern[a]

Eddy type	Season	P_{10}(Cor)	Median(Cor)	p(Cor>0.71)
Median Pattern				
ACE	Winter	−0.19	0.38	7.3%
ACE	Summer	−0.31	0.28	3.0%
CE	Winter	−0.16	0.33	5.4%
CE	Summer	−0.19	0.39	10.4%
SOM Pattern				
ACE	Winter	0.42	0.70	49.0%
ACE	Summer	0.31	0.59	28.2%
CE	Winter	0.45	0.73	56.6%
CE	Summer	0.34	0.65	38.8%

[a]Cor is the spatial correlation between each individual eddy CHL' pattern and the median pattern (upper part of the table) or the best matching SOM pattern (lower part of the table). p(Cor>0.71) corresponds to the fraction of eddies having spatial correlation exceeding 0.71. That parameter together with the median value and the 10th percentile (P_{10}) of the correlation coefficients Cor are listed for both ACEs and CEs during winter (June/July/August) and summer (December/January/February).

The considerable variability in CHL' patterns that are hidden by the median are highlighted by the SOM analysis performed over winter (Figures 4 and 5). The relative frequency of each SOM pattern is included in Figures 4 and 5 and shows that all patterns are represented in the data. The SOM patterns capture a reasonable fraction of the eddy CHL' variability. For instance, 49% of ACEs and 57% of CEs have one SOM pattern (the best one) that captures more than 50% of the observed spatial variance (Table 1). Moreover, the patterns presented in Figures 4 and 5 show good (median) spatial correlations (respectively 0.70 and 0.73 for
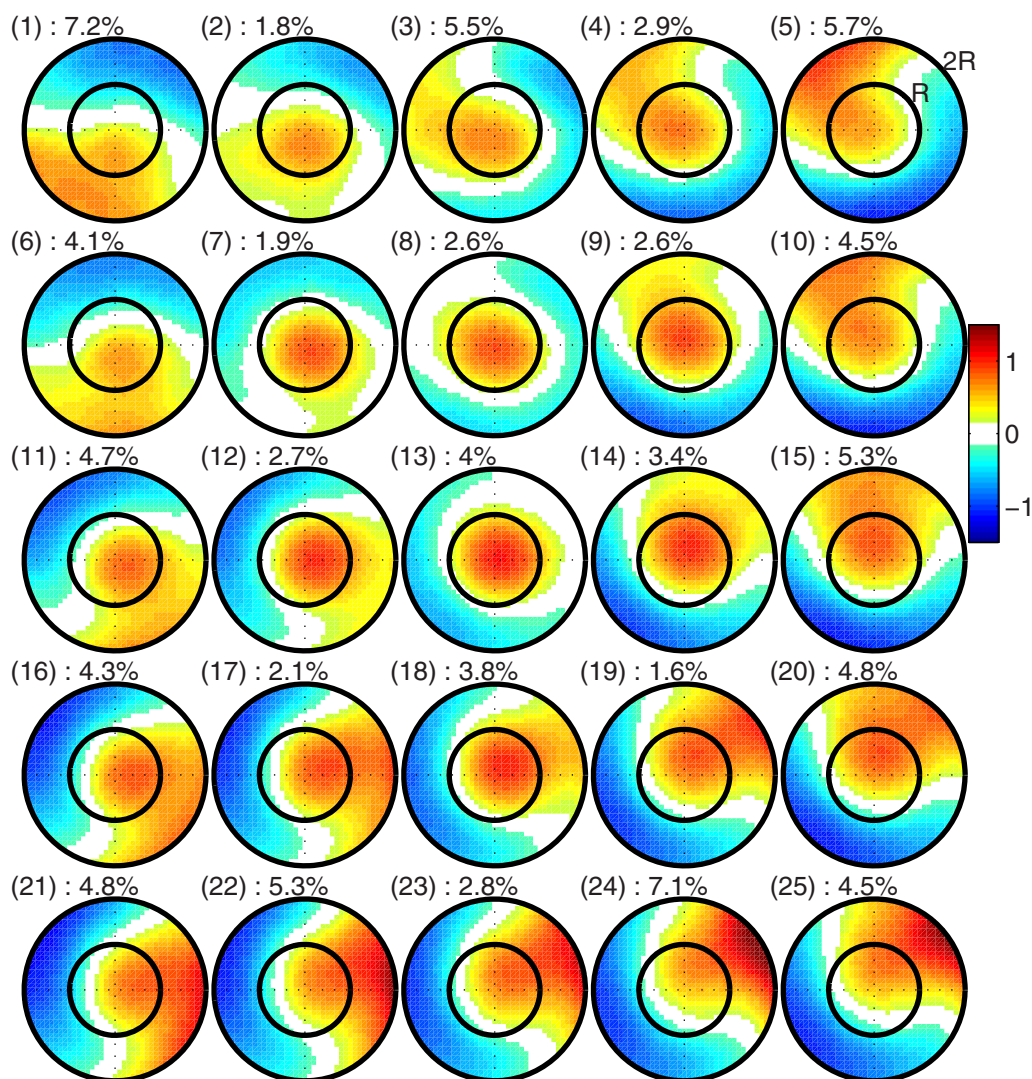
Figure 4. SOM for CHL' patterns within ACEs in winter (June/July/August) in Region A. The relative frequency of appearance of each pattern is shown above each pattern (their sum equal 100%). Inner and outer circles coincide with r/R=1 and r/R=2. *N.B.*: more similar spatial patterns are in closer proximity and more dissimilar patterns are further apart (i.e., the four corners of the SOM represent the most extreme patterns, with a smooth continuum in between).

ACEs and CEs) with individual eddy CHL' patterns. Although the SOM analysis performed better during winter, it still captures a reasonable fraction of the eddy variability during summer (Table 1).

While the pattern on the top-left corner of Figure 4 for ACEs exhibits higher CHL' values to the SW of the eddy centre, the three other corners (top-right, bottom-right, and bottom-left) exhibit higher CHL' values respectively to the NW, to the NE and to the SE of the eddy centre. Similarly, for CEs, while the pattern on the top-left corner of Figure 5 exhibits lower CHL' values to the NE of the eddy centre, the three other corners (top-right, bottom-right, and bottom-left) exhibit lower CHL' values respectively to the SE, to the SW, and to the NW of the eddy centre. In between the four corners of Figures 4 and 5, there is a continuum of change across the two-dimensional SOM array. Consequently, patterns close to the centre of the SOM arrays exhibit higher CHL' values close to the eddy centre for ACEs, and lower values close to the eddy centre for CEs.

The most frequent pattern for ACEs is pattern 1 (7.2%), where higher CHL' values are to the SW of the eddy centre (Figure 4). This pattern is most common at 75°E where it occurs 24% of the time (Figure 6). For CEs, the most common pattern is pattern 5 (7.6%), where lower CHL' values are to the SE (Figure 5). This pattern is most common at 90°E where it occurs 23% of the time (Figure 6). The SOM analysis confirms that the
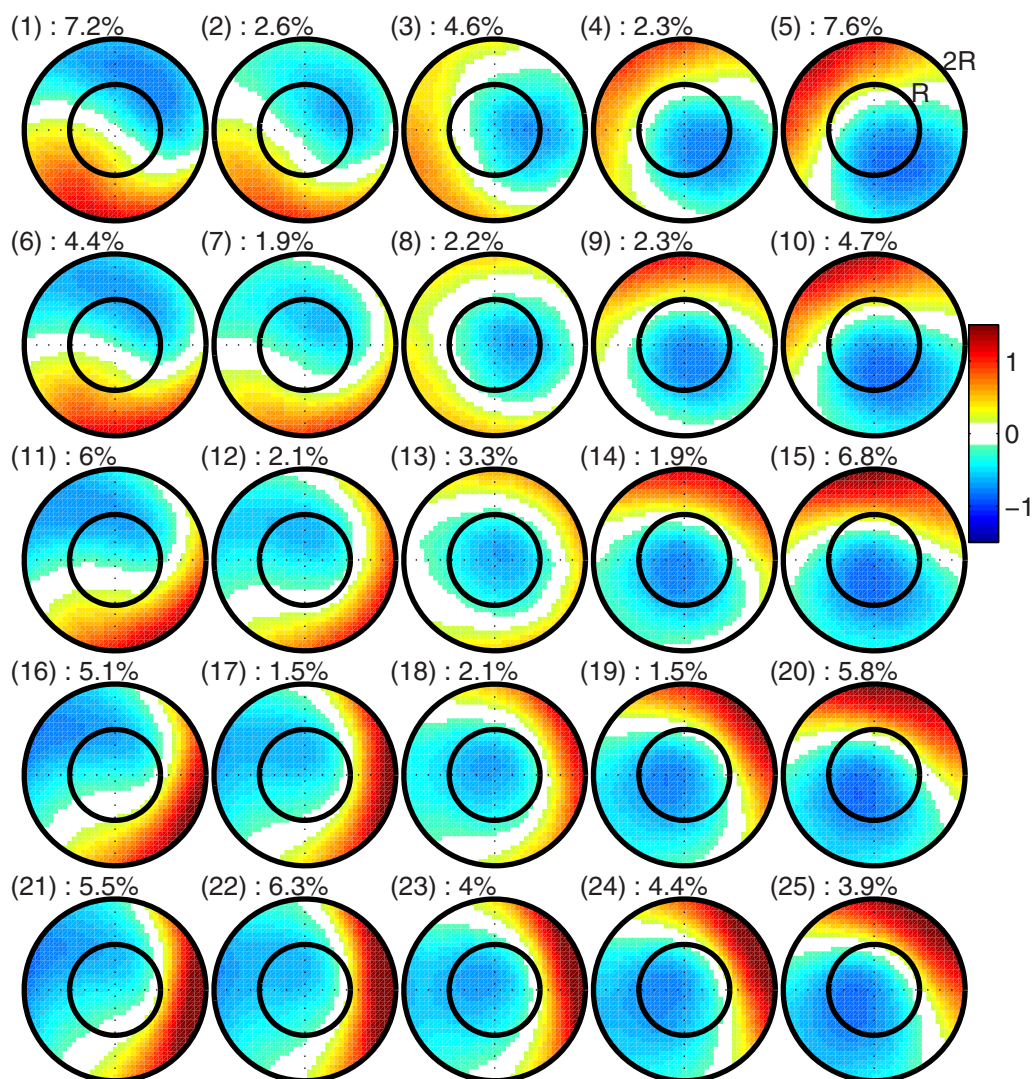
Figure 5. SOM for CHL' patterns within CEs in winter (June/July/August) in Region A. The relative frequency of appearance of each pattern is shown above each pattern (their sum equal 100%). Inner and outer circles coincide with r/R=1 and r/R=2. *N.B.*: more similar spatial patterns are in closer proximity and more dissimilar patterns are further apart (i.e., the four corners of the SOM represent the most extreme patterns, with a smooth continuum in between).

composite patterns of median CHL' (Figure 3) are rare. Only a few patterns (patterns 7, 8 and 13 on Figure 4 for ACEs and patterns 8 and 13 on Figure 5 for CEs) look similar to the patterns in Figure 3. Those patterns, presenting a CHL anomaly with a circular shape centred in the eddy centre, only occurred 8.5% of the time for ACEs and 5.5% for CEs (Figures 4 and 5). Although they can be observed over the whole Region A (Figure 6), they are predominant from 80 to 95°E for CEs. For ACEs, while pattern 8 is predominant west of 90°E, pattern 7 is more common around 90°E and pattern 13 is more common around 100°E.

Patterns with higher CHL' to the east of eddies are more common toward the east of Region A. This is the case for patterns 11, 12, 16–18 and 21–24 for both ACEs and CEs (Figure 6). On the contrary, patterns 1–5 for ACEs and 3–5, 9, 10 and 15 for CEs are more common to the west of Region A.

Despite the variability in eddy CHL' patterns, 45% of ACEs (patterns 2–4, 6–9, 11–15, 18) and 15% of CEs (patterns 9, 13–14, 18–19, 23) correspond to a SOM pattern having a higher absolute CHL' value close to the eddy centre ($r/R \leq 0.5$) (Figures 4 and 5). Similarly, 57% of ACEs (patterns 2–4, 6–9, 11–18, 20) and 64% of CEs (patterns 2–5, 7–10, 12–15, 18–20, 23–25) correspond to a SOM pattern having a higher absolute CHL' value within the eddy centroids ($r/R \leq 1$). Those CHL' patterns with higher absolute values located in the vicinity of the eddy centre can be observed over the whole of Region A (Figure 6).
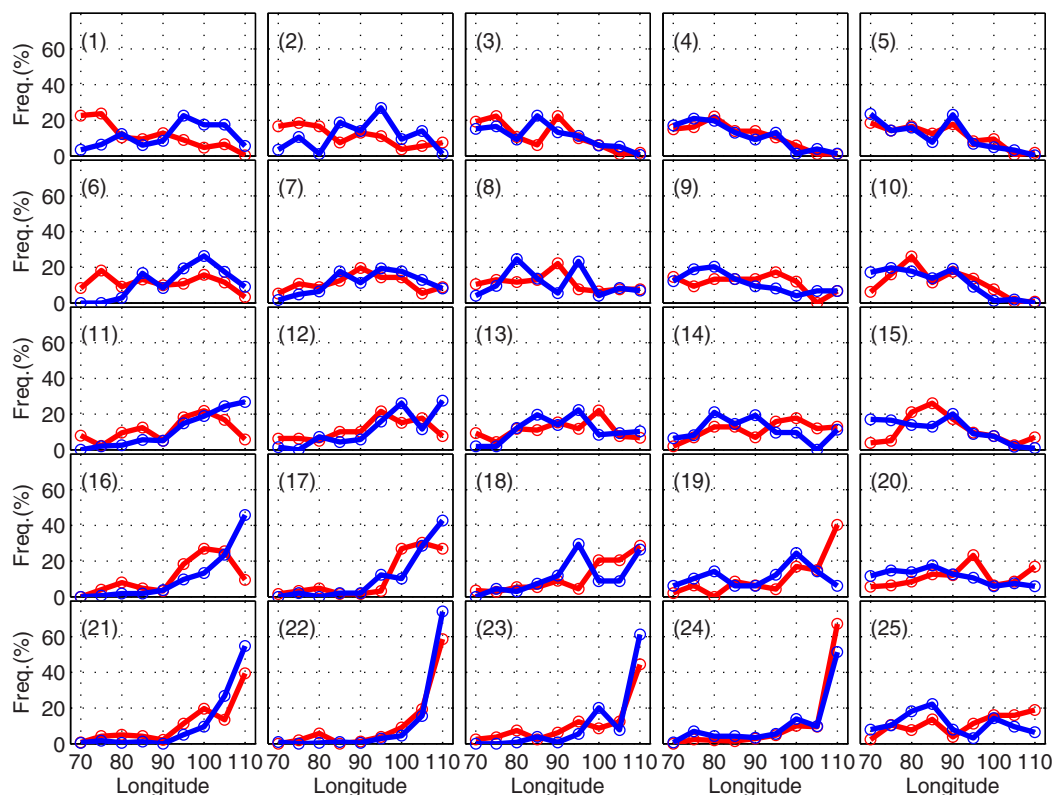
Figure 6. Frequency (%) of appearance of each 25 SOM patterns (computed in winter (June/July/August) for years 1998–2010 over Region A) along longitudes for CEs (blue) and ACEs (red).

3.3. Mixed Layer Entrainment: Eddy-Induced Ekman Pumping Versus Seasonal MLD Change

In this section we estimate the mixed layer vertical fluxes of nitrate (Equation (2)) to assess the relative contribution of eddy-induced Ekman pumping, and seasonal change in MLD, on the CHL/eddy relationship. The MLD within ACEs is significantly deeper than within CEs in the South Indian Ocean over Region B (Figure 7). Furthermore, the rate of change in the MLD during the strongest mixing phase is faster in ACEs (Figure 8a). From May to August, when the mixed layer is deeper, the difference of MLD rate of change between ACEs and CEs (i.e., $\frac{\partial h(ACE)}{\partial t} - \frac{\partial h(CE)}{\partial t}$) is between 29 and 64 cm d^{-1}. In comparison, the difference of eddy-induced Ekman pumping in ACEs and CEs (i.e., $w_{-h}(ACE) - w_{-h}(CE)$) reaches only 13.7 cm d^{-1} on average for the Leeuwin Current eddies (cf. section 2.3). Therefore, from May to August the anomaly of entrainment rate between ACEs and CEs is dominated by the MLD rate of change (i.e., $\frac{\partial h(ACE)}{\partial t} - \frac{\partial h(CE)}{\partial t} > w_{-h}(ACE) - w_{-h}(CE)$). During those months at least, corresponding to the highest CHL anomalies in eddies, the seasonal change of MLD has a greater impact on the nutrient flux into the mixed layer, and therefore probably also the surface CHL anomaly, than the eddy-induced Ekman pumping.

The deeper MLD in ACEs implies that they will penetrate deeper below the nutricline into higher nitrate concentrations than CEs (Figure 7). The term $\bar{C} - C_{-h}$ of Equation (2) would therefore be bigger in ACEs than in CEs, inducing enhanced nitrate fluxes in the mixed layer of ACEs. Consequently, the nitrate flux in the mixed layer appears to be dominated by the seasonal change in MLD (Figure 8b). Over the course of one climatological year, the time-integrated upwelling flux induced by an eddy-induced Ekman upwelling of 7.8 cm d^{-1} (cf. section 2.3) is 3.2 times lower than the anomaly (between ACEs and CEs) of the time-integrated nitrate flux induced by the change in MLD (Figure 8b).

The peak in the time-integrated nitrate flux, due to the change in MLD, coincides in time with the peak in the CHL anomaly, while the time-integrated eddy-induced Ekman upwelling flux peaks later in November (Figure 8b). On average over the Region B, the CHL difference between ACEs and CEs at the surface peaks in July, increasing from less than 10^{-3} mg m^{-3} in March to 0.014 mg m^{-3} (Figure 2). The CHL anomaly in July is equivalent to a range of values of phytoplankton nitrogen biomass anomaly of between 0.011 and 0.031 mmol m^{-3} (Figure 8b). This corresponds to an average anomaly of rate of change of nitrogen biomass

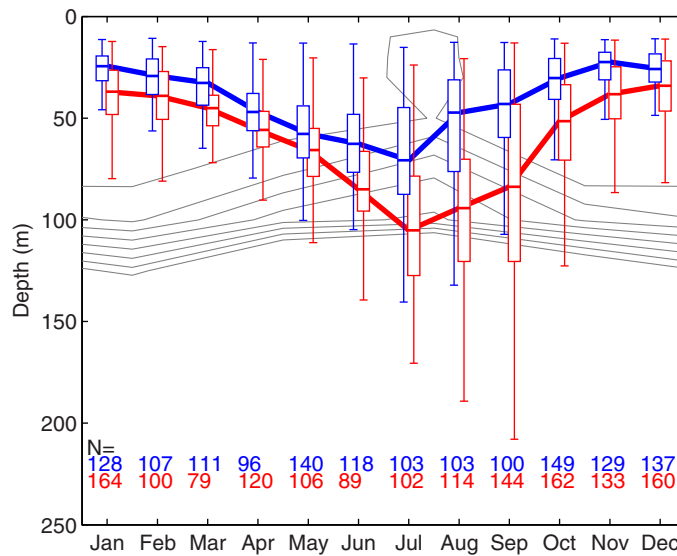**Figure 7.** Climatology of MLD in CE (blue) and ACE (red) interiors (r/R≤1) from ARGO floats in Region B. The number N of ARGO floats used for each month is reported. The thin gray lines correspond to the NO$_3$ mean seasonal contours (from World Ocean Atlas 2009) ranging from 0.3 to 1 mmol m^{-3}. In the box-plot, the rectangular box is delimited by the lower quartile (Q1) and the upper quartile (Q3), while the median is represented inside the box by a straight line. Whiskers are drawn to the extreme values that are inside the fences lying at Q1 − 1.5×(Q3–Q1) and Q3 + 1.5×(Q3–Q1). Lines join median values.

of between 9×10^{-5} and 2.3×10^{-4} mmol m^{-3} d^{-1} from March to July. Over the same period, the nitrate flux anomaly between ACEs and CEs due to a change in MLD averages 9×10^{-4} mmol m^{-3} d^{-1}, while the eddy-induced Ekman pumping flux in ACEs averages 10^{-4} mmol m^{-3} d^{-1}.

3.4. Eddies and Water Column Stability

During summer in Region B, the shallow mixed layer sits just above the more stable water (i.e., higher N^2) observed throughout the year, both in ACEs and CEs (Figure 9). From March to July, when the mixed layer deepens, the shallow stratification breaks down. The lower stability observed below the MLD in winter highlights the impact of mixing on the water column.

Restratification of the water column is initiated from August, and by November the mixed layer reaches its average summer depth. This scenario is highlighted for both ACEs and CEs on Figure 9, and is also observed outside the eddies (not shown).

The difference of seasonal MLD change in ACEs and CEs is reflected in the seasonal water column stabilities in eddies (Figure 9). Near the surface, the overall squared buoyancy frequency N^2 is lower in ACEs than in CEs. ACEs are less stable than CEs from 0 to 60 m depth during summer, and the stability anomaly even reaches ~100 m depth during winter.
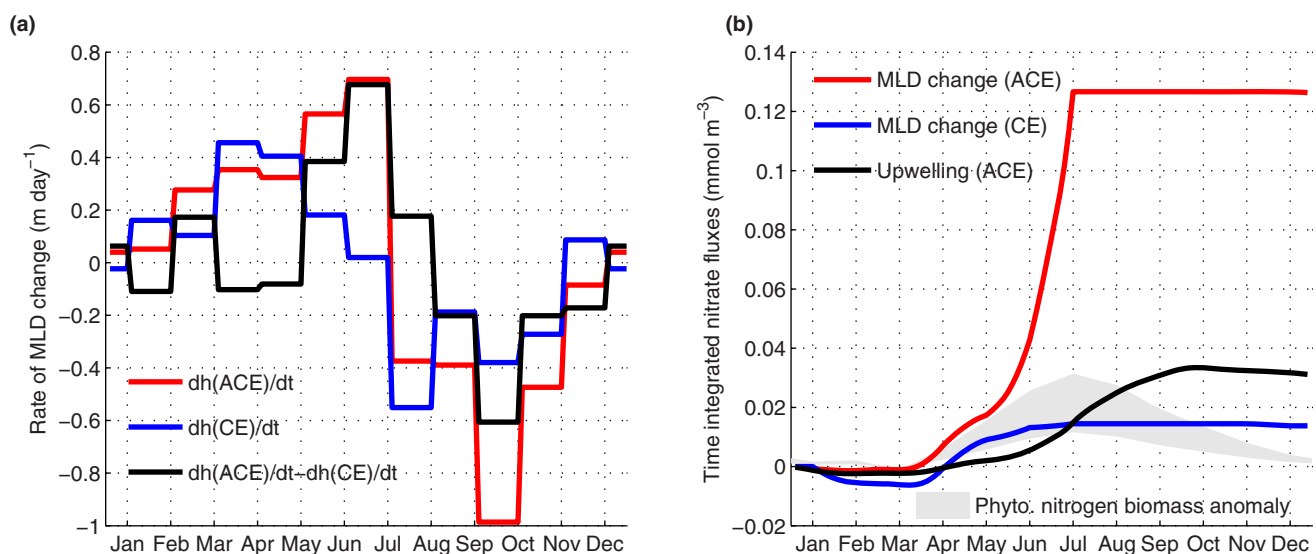

Figure 8. (a) Monthly MLD rate of change (m d^{-1}) for ACEs (red) and CEs (blue) calculated from ARGO floats in Region B (for r/R≤1). The black line is the difference between the red line and the blue line. (b) Time integrated nitrate flux (mmol m^{-3}) in the mixed layer due to MLD change in ACEs (red line) and in CEs (blue line) and eddy-induced Ekman pumping in ACEs (black line). The grey shaded area corresponds to the anomaly of phytoplankton nitrogen biomass (mmol m^{-3}) between ACEs and CEs (computed from a range of likely carbon-to-chlorophyll ratios).
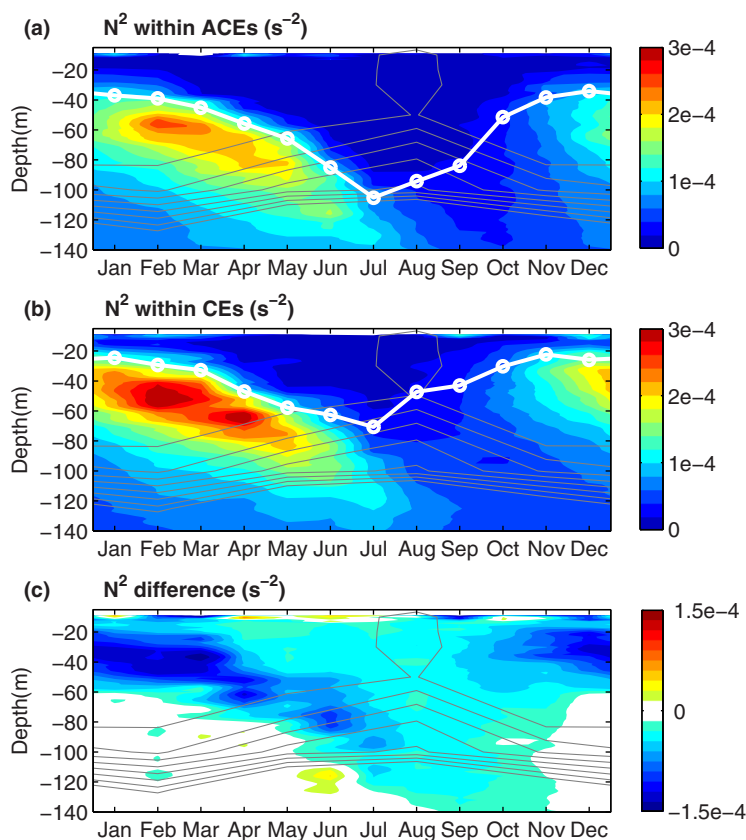
Figure 9. Squared buoyancy frequency (shading) and median MLD (white lines with circles) within ACEs (a) and CEs (b) in Region B (for r/R≤1). (c) Squared buoyancy frequency difference between ACEs and CEs. The grey lines correspond to the NO_3 mean seasonal contours ranging from 0.3 to 1 mmol m^{-3}.

4. Discussion

Here we show that ACEs exhibit higher surface CHL concentration than CEs across the entire South Indian Ocean basin (from 20 to 28°S), particularly in winter when the seasonal CHL is at its maximum. The variance explained by the median pattern of CHL is small and multiple patterns are needed to characterize the CHL variability. The complexity of the CHL patterns within eddies illustrated by the SOMs suggests that multiple mechanisms are responsible for the anomalous eddy/chlorophyll relationship.

4.1. Mechanisms
4.1.1. Meridional Advection of CHL Gradient
The large-scale horizontal CHL gradient appears to be a major component of the CHL eddy patterns in winter. The meridional advection of a CHL gradient, generating a CHL anomaly along the eddy edge [*Chelton et al.*, 2011a], can explain some of the SOM patterns. This is, for instance, the case for patterns 1 and 6 of the SOM for CEs (Figure 5). That process alone should not elevate CHL values in ACEs. However, the mechanism described by *Killworth et al.* [2004] for Rossby waves could explain how the anomaly generated along the eddy edges could move to the eddy centre, for the less nonlinear of the eddies (i.e., those having a rotational speed to propagation speed ratio U/C close to 1) [*Chelton et al.*, 2011b]. In their study, *Killworth et al.* [2004] explained that meridional advection of the CHL gradient, combined with slow relaxation, can lead to CHL anomalies in the centre of eddies in phase with SSH anomalies. The relaxation is considered slow when the time needed for a CHL anomaly to disappear due to ambient physical or biogeochemical forcing is long (e.g., >>20 days at high latitudes and >>150 days at low latitudes). That process may be reflected in pattern 5, and its neighbours, of the SOM for ACEs (Figure 4). However, only a small portion of eddies considered in this study have a low nonlinearity parameter U/C. Over Region B for instance, only 10% of the eddies have a nonlinearity parameter U/C<1.5 and 18% have U/C<2.
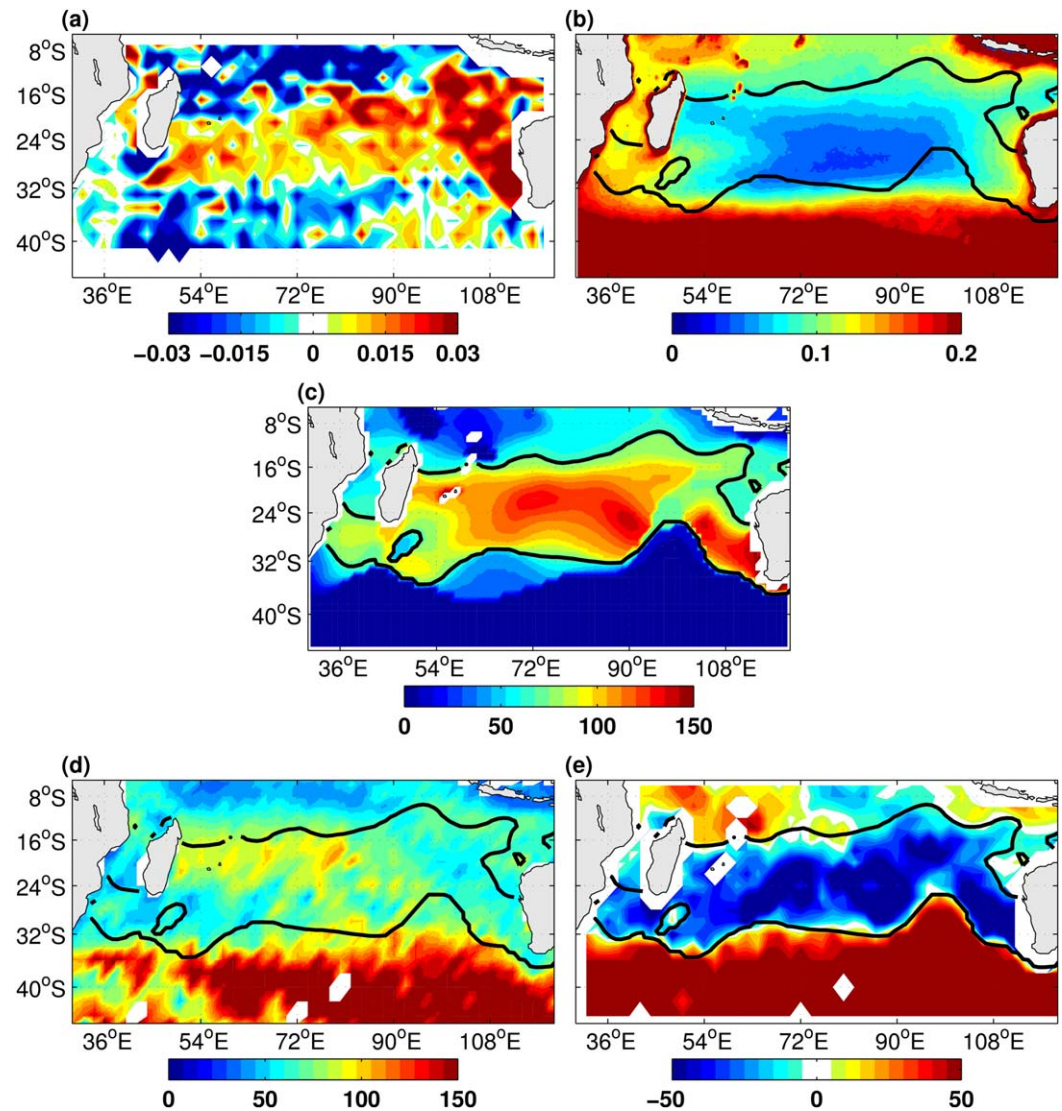
Figure 10. CHL, MLD and nutricline depth in the South Indian Ocean during June/July/August. (a) Difference between surface CHL in ACEs and in CEs (mg m^{-3}). (b) Mean CHL (mg m^{-3}). (c) Mean depth (m) of the nutricline (define as the 1 mmol m^{-3} of NO$_3$ contour). (d) Mean MLD (m). (e) Difference between the MLD and the nutricline depth (m). The black line highlights the 70 m depth contour of the nutricline.

4.1.2. Eddy Generation and Propagation

The propagation of the CHL anomaly, entrained within eddies, from the Leeuwin Current region to the central South Indian Ocean has been suggested to explain the CHL/SSH relationship in the South Indian Ocean [*Brewin et al.*, 2012; *Moore et al.*, 2007]. In the SOM analysis, some patterns are consistent with westward propagation of higher CHL water from the shelf (e.g., patterns 16–18 and 21–24 on Figure 4). Those patterns are mostly observed along the west coast of Australia (Figure 6). Importantly, there is no evidence of a time lag between the CHL seasonal cycle inside and outside eddies in our analysis. Such a lag would be expected if the winter CHL bloom in the Leeuwin Current was propagating westward via eddies. The peak season of CHL within eddies would then depend on the distance from the shelf. We therefore suggest that the impact of propagating shelf eddies is restricted to the eastern part of the basin. This is in agreement with *Greenwood et al.* [2007] and *Dietze et al.* [2009] who suggested that, once separated from the shelf, CHL anomalies resulting from entrainment of Leeuwin Current water in ACEs, would be maintained for less than a year, which is not long enough for an eddy to cross the entire South Indian Ocean basin [*Chelton et al.*, 2011b].

A similar mechanism related to the generation of eddies in regions of higher CHL could also be evoked for eddies forming offshore. *Gaube et al.* [2013] suggested that, due to the CHL increasing to the north (north of 28°S, Figure 10b), and the generally eastward flowing upper-ocean currents in the eastern part of the South Indian Ocean, ACEs that form offshore entrain water with higher CHL during generation. On the contrary, CEs that form offshore are likely to entrain water with lower CHL. Although there is no formal evidence that this process is taking place, the patterns 4–5 and 9–10 of the SOM for ACEs (Figure 4) are broadly consistent with this mechanism.

4.1.3. Eddy-Induced Ekman Pumping

Gaube et al. [2013] suggested that in the South Indian Ocean the CHL anomalies within ACEs result from an input of nutrient as a result of eddy-induced Ekman pumping. Eddy-induced Ekman pumping has previously been suggested as a mechanism to explain enhanced nutrient supply to the surface within ACEs in the North Atlantic [*Martin and Richards*, 2001; *McGillicuddy et al.*, 2007]. However, the relative impact on nutrient supply of eddy-induced Ekman pumping versus submesoscale processes is in debate [*Mahadevan et al.*, 2008; *McGillicuddy et al.*, 2008].

Eddy-induced Ekman pumping is consistent with SOM patterns having a higher absolute anomaly located in the eddy centre, and especially patterns 7, 8, and 13 for ACEs (Figure 4). However, we showed that during the period of higher CHL anomalies, the seasonal MLD rate of change difference between ACEs and CEs in the South Indian Ocean is much greater than the vertical eddy-induced Ekman pumping velocities. Thus, the vertical nitrate flux difference between ACEs and CEs is dominated by the MLD change flux. We also showed that the nitrate flux of eddy-induced Ekman pumping appears to be out of phase with the rate of change of CHL anomaly between ACEs and CEs. The eddy-induced Ekman pumping nitrate flux reaches a peak in July, when the mixed layer is the deepest and the CHL anomaly rate of change is null (i.e., the CHL anomaly is the highest). We conclude that eddy-induced Ekman pumping does not seem to be supported as the dominant mechanism to explain the observed elevated CHL at the centre of ACEs compared to CEs and may only play a minor role in the nutrient budget of ACEs.

Due to lack of nitrate data within eddies in the South Indian Ocean, we could not account, in the nitrate budget, for: (i) the difference of nitrate profiles between ACEs and CEs; and (ii) the impact of the eddy-induced Ekman pumping on the concentration below the mixed layer (C_{-h}). We acknowledge that this is a limitation of our analysis and that further work is needed to assess the nitrate budget within eddies more accurately.

4.1.4. Seasonal MLD Change

Given that the most significant differences between CHL in ACEs and CEs is in winter at the time of maximum seasonal CHL, we hypothesize that processes amplifying the seasonal CHL maximum in eddies could be partly responsible. The modulation of the seasonal cycle of the MLD by mesoscale eddies could contribute to elevated CHL in ACEs.

In a nutrient-limited and relatively "shallow" MLD environment like the South Indian Ocean, injection of nutrients into the MLD is likely to enhance CHL. The seasonal increase of surface CHL is observed in winter when the mixed layer deepens and overlays the nutricline. Observations show that, in the South Indian Ocean, this deepening of the mixed layer is more important in ACEs than in CEs, which enhances the nutrient flux into the mixed layer in ACEs.

In general, changes in the MLD are due to both turbulent vertical mixing and adiabatic processes associated with the vertical stretching terms and/or the eddy-pumping. Eddy-pumping, shallowing the isopycnals in ACEs, cannot be responsible for deeper MLD in ACEs in winter. In addition, the eddy kinetic energy, which may be used as a proxy for the intensity of mesoscale eddies and therefore the deepening of isopycnals in ACEs, peaks in summer in the South Indian Ocean [*Jia et al.*, 2011]. These findings suggest, therefore, that turbulent vertical mixing is the main contributor of the seasonal MLD change within eddies. In fact, we showed that surface water is less stable in ACEs and more stable in CEs than the surrounding waters of the South Indian Ocean, which may lead to deeper winter convective mixing in ACEs. Weak preexisting stratification in ACEs has already been shown to contribute to deeper MLD in other parts of the ocean [*Kouketsu et al.*, 2012]. In the South Indian Ocean, deeper MLD and quicker rates of MLD change in ACEs are due to weak preexisting stratification all year round, allowing more efficient convective mixing in response to negative net heat flux at the surface.

This enhanced convective mixing might fuel phytoplankton production in ACEs both by increasing the nutrient entrainment rate and by reaching the nutricline earlier in the season or deeper during the peak season. During the increasing phase of eddy CHL anomaly, we estimated the nitrate flux anomaly between ACEs and CEs induced by mixed layer deepening to be 4–10 times higher than the anomaly of phytoplankton nitrogen biomass rate of change. This rate of change can be considered as the minimum nitrate flux needed to produce the CHL anomaly if all nitrate was used up by phytoplankton and no loss of phytoplankton (through grazing, settling, mortality, etc.) occurred. Thus, the nitrate flux appears sufficient to allow for phytoplankton loss processes or growth inefficiency, making the MLD anomaly in eddies a plausible mechanism to explain the CHL anomaly.

The region where winter ACEs exhibit higher levels of surface CHL than CEs matches the region with low CHL values and relatively deep nutricline (Figures 10a–10c). This region is also delimited to the south by deeper winter MLD (Figure 10d) and coincides with an area where the mean MLD is shallower than the nutricline (Figure 10e). We therefore suggest that, more generally, the modulation of the MLD by mesoscale eddies could impact the CHL seasonal cycle in oligotrophic regions where the MLD is shallower than the nutricline.

4.1.5. Submesoscale Processes

Other mechanisms could lead to CHL anomalies being higher in ACEs than in CEs, with the strongest absolute anomaly being localized in the eddy centre. Large (up to 35 m d^{-1}), submesocale, vertical velocities have been observed around the perimeter of a Leeuwin Current ACE [*Paterson et al.*, 2008], and have previously been suggested to maintain ACE phytoplankton communities for more than five months through injection of nutrients into the eddy boundary [*Moore et al.*, 2007]. The convergent nature of forming ACEs could then allow CHL anomalies generated along the eddy edges to become entrained toward the eddy centre. Using a numerical model, *Lévy and Klein* [2004] demonstrated that ACEs can have higher CHL in their centre due to submesoscale processes. We were unable to find any evidence of submesoscale features, although they could have been hidden in some of the SOM patterns. We also acknowledge that the statistical approach we used, together with the spatiotemporal filtering applied to the CHL database, is not suited to track small-scale, short-period, variability.

4.2. Eddies or Rossby Waves

The positive correlation found off Western Australia between S$\tilde{S}$H and C$\tilde{H}$L suggested that the relationship between SSH and CHL could be a consequence of the mesoscale activity. Upwelling (and downwelling) induced by propagating baroclinic Rossby waves can enhance (and dampen) primary production in the Tropical Indian Ocean) [e.g., *Cipollini et al.*, 2001; *Currie et al.*, 2013; *Kawamiya and Oschlies*, 2001; *Ma et al.*, 2014]. Consequently a pattern of negative correlation between CHL and SSH is observed in this region [*Brewin et al.*, 2012]. This pattern is reduced when CHL and SSH are high-pass filtered along longitude (Figure 1). This gives us confidence that the Rossby wave impact on the CHL field is mostly removed in our analysis in Figure 1. In contrast, the positive correlation between SSH and CHL off Australia is enhanced after high-pass filtering, providing some support for the hypothesis that the relationship between SSH and CHL is caused by the eddy dynamics.

4.3. Utility of SOMs

Since its introduction to the oceanography community by *Richardson et al.* [2003], SOMs have become increasingly popular and have been used in a large range of fruitful applications [*Liu and Weisberg*, 2011]. In our study, the SOM analysis provided a more detailed picture and interpretation of the variability of CHL patterns in eddies. Median patterns (Figure 3) proved to be misleading, since they suggested that CHL anomalies were constrained to the eddy centre, implying that mesoscale vertical processes were primarily responsible. In contrast, the SOM analysis highlighted the variety and complexity of the CHL patterns that exist within eddies and the importance of the horizontal CHL gradient, suggesting that multiple processes were involved.

For comparison, we also conducted a more conventional Empirical Orthogonal Function (EOF) analysis (see Appendix A). In agreement with the SOM analysis, the EOF showed that many modes were required to characterize the CHL variability for ACEs. It also showed that the EOF mode with the greatest explained variance was not consistent with the median analysis. Further, the first three spatial patterns of the EOF were similar to some of the SOM patterns. However, the EOF modes were difficult to interpret. EOF analysis identifies

patterns, but they are not fixed and can vary between a positive and a negative expression (principal components can oscillate in sign). For example, the third EOF in Figure A1 produces a pattern of high chlorophyll in the eddy centre but this pattern is reversed 38% of the time when multiplied by negative principal component values.

We ultimately chose to use the SOM analysis because it was more intuitive and easier to interpret than the more conventional EOF analysis. SOM has previously been shown to be more reliable in retrieving complex patterns in many oceanographic situations [e.g., *Liu et al.*, 2006; *Reusch et al.*, 2005]. We confirm its utility in pattern identification in satellite imagery.

5. Conclusion

In the South Indian Ocean, distinct differences between CE and ACE CHL levels are observed, and are phase locked to the seasonal cycle. Significantly higher values of CHL in ACEs than in CEs are observed across the whole South Indian Ocean basin during winter, when the seasonal CHL is at its maximum. There are several key findings from our study. First, CHL anomalies generated in Leeuwin Current eddies are not propagated very far offshore and therefore cannot explain the unusual CHL/eddy relationship observed over the whole basin. Second, the SOM analysis, performed over the eddy CHL patterns during winter, highlighted that various CHL patterns lead to higher concentrations of CHL in ACEs than in CEs. This suggests that a variety of processes jointly contribute to the overall increase of surface CHL in ACEs, and decrease in CEs. Third, a few of the SOM patterns (those presenting a circular CHL anomaly restricted to the eddy centre) suggest the existence of vertical processes acting at the eddy centre. Lastly, our study provides evidence that eddy Ekman pumping is unlikely to be the main vertical forcing of the positive CHL anomaly observed in ACEs. Instead, the seasonal modulation of the MLD is proposed to be the dominant vertical mechanism, and capable of explaining the difference between CHL in ACEs and CEs in winter, at the time of maximum seasonal phytoplankton biomass. It is however premature to quantify the impact of the convective mixing alone.

Further studies, perhaps for example using coupled physical-biogeochemical models, may be needed to quantify the respective impact of the various processes listed previously on the anomalous behavior in the South Indian Ocean. However, there are relatively few biogeochemical data available within the oligotrophic South Indian Ocean, even fewer within eddies. A first set of biogeochemical data has recently been acquired within eddies using profiling floats (*Tom Trull*, pers. com.), which may help to parameterize a suitable model.

Appendix A: EOF Analysis of CHL Patterns

We performed an Empirical Orthogonal Function (EOF) analysis [*Legendre and Legendre*, 2012] to decompose the surface CHL' patterns within eddies. The EOF analysis is performed directly on CHL' without removing the mean structure (similar to the approach employed for the SOM analysis). Here we present the spatial patterns of the EOFs explaining more than 10% of the CHL' variability (referred to as EOF1, EOF2, etc.), together with histograms of their associated principal component (referred to as PC1, PC2, etc.). For discrete longitudinal regions we also provide the probability of the PCs to be positive, negative, greater than 1 standard deviation or lower than −1 standard deviation.

The EOF analysis performed over the CHL' patterns in ACEs in winter shows 3 main modes of variability explaining respectively 23, 17.9 and 11% of the total variance (Figure A1a). None of the subsequent EOF spatial patterns seem to be spatially meaningful (not shown) and the 4th EOF mode explains less than 6.5 % of the total variance. The principal component of the first EOF is positive for 78% of the ACEs (Figure A1a). Further, PC1 exhibits most of the higher positive values closer to the West Australian coasts (Figure A1a). EOF1 is therefore led by eddies located in the east of Region A. PC2 is globally positive in 56% of cases (Figure A1b). To the west of the domain PC2 is however more frequently negative. Therefore, EOF2 presents more CHL' patterns with a SE-NW gradient toward the west side of the domain (opposite sign to the pattern presented on Figure A1a) and more patterns with a NW-SE gradient toward the east side of the domain. Finally, PC3 is positive for 62% of eddies over Region A (Figure A1b). EOF3 highlights a higher absolute anomaly of CHL located in the eddy centre. This anomaly tends to be predominantly positive over the whole domain, except east of 105°E, where a central negative anomaly pattern is more common.
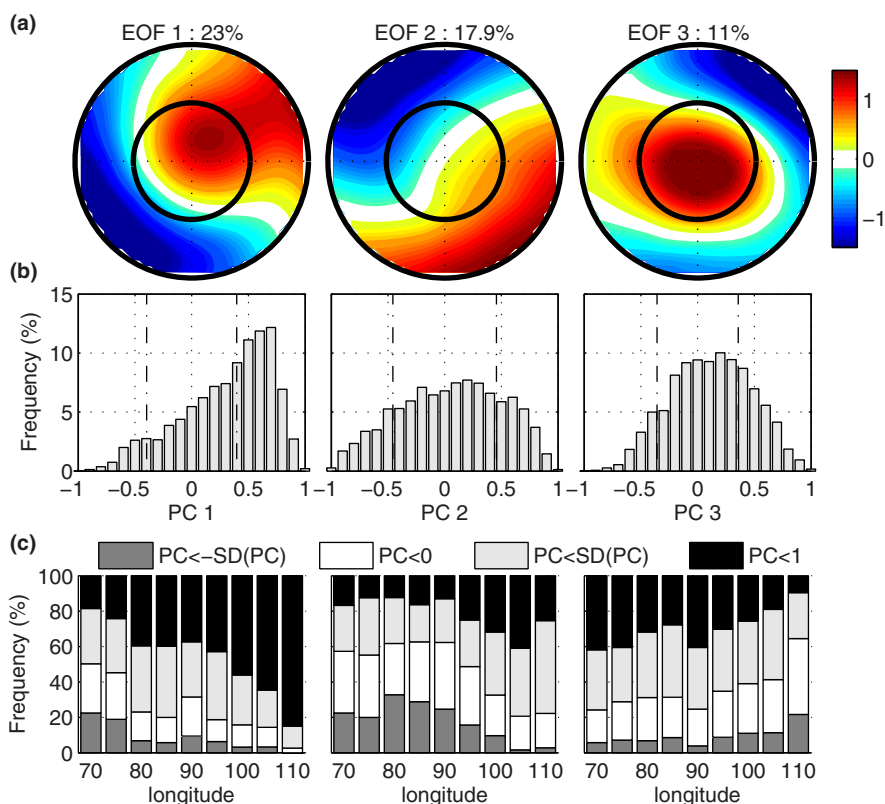
Figure A1. EOF decomposition for CHL' patterns within ACEs in winter (June/July/August) in Region A. (a) Spatial patterns of the first three EOFs. The fraction of the variance explained by the EOF is indicated above each pattern. Inner and outer circles coincide with r/R=1 and r/R=2. (b) Histograms of associated principal components. Black dash lines indicate ±1 standard deviation (SD). (c) Probability (%) of the principal component to be positive, negative, greater than 1 standard deviation or lower than −1 standard deviation for discrete longitudes of Region A.

References

Brewin, R. J. W., T. Hirata, N. J. Hardman-Mountford, S. J. Lavender, S. Sathyendranath, and R. Barlow (2012), The influence of the Indian Ocean Dipole on interannual variations in phytoplankton size structure as revealed by Earth Observation, *Deep Sea Res. Part II*, *77–80*, 117–127, doi:10.1016/j.dsr2.2012.04.009.

Campbell, J. W. (1995), The lognormal distribution as a model for bio-optical variability in the sea, *J. Geophys. Res.*, *100*(C7), 13,237–13,254, doi:10.1029/95JC00458.

Caniaux, G., and S. Planton (1998), A three-dimensional ocean mesoscale simulation using data from the SEMAPHORE experiment: Mixed layer heat budget, *J. Geophys. Res.*, *103*(C11), 25,081–25,099.

Chelton, D. B., P. Gaube, M. G. Schlax, J. J. Early, and R. M. Samelson (2011a), The influence of nonlinear mesoscale eddies on near-surface oceanic chlorophyll, *Science*, *334*(6054), 328–332, doi:10.1126/science.1208897.

Chelton, D. B., M. G. Schlax, and R. M. Samelson (2011b), Global observations of nonlinear mesoscale eddies, *Prog. Oceanogr.*, *91*(2), 167–216, doi:10.1016/j.pocean.2011.01.002.

Cipollini, P., D. Cromwell, P. G. Challenor, and S. Raffaglio (2001), Rossby waves detected in global ocean colour data, *Geophys. Res. Lett.*, *28*(2), 323–326.

Currie, J. C., M. Lengaigne, J. Vialard, D. M. Kaplan, O. Aumont, S. W. A. Naqvi, and O. Maury (2013), Indian Ocean Dipole and El Niño/Southern Oscillation impacts on regional chlorophyll anomalies in the Indian Ocean, *Biogeosci. Discuss.*, *10*(3), 5841–5888, doi:10.5194/bgd-10-5841-2013.

de Boyer Montégut, C., G. Madec, A. S. Fischer, A. Lazar, and D. Iudicone (2004), Mixed layer depth over the global ocean: An examination of profile data and a profile-based climatology, *J. Geophys. Res.*, *109*, C12003, doi:10.1029/2004JC002378.

Dietze, H., R. Matear, and T. Moore (2009), Nutrient supply to anticyclonic meso-scale eddies off western Australia estimated with artificial tracers released in a circulation model, *Deep Sea Res. Part I*, *56*(9), 1440–1448, doi:10.1016/j.dsr.2009.04.012.

Feng, M., L. J. Majewski, C. B. Fandry, and A. M. Waite (2007), Characteristics of two counter-rotating eddies in the Leeuwin Current system off the Western Australian coast, *Deep Sea Res.*, *54*(8-10), 961–980, doi:10.1016/j.dsr2.2006.11.022.

Garcia, H. E., R. A. Locarnini, T. P. Boyer, J. I. Antonov, M. M. Zweng, O. K. Baranova, and D. R. Johnson (2010), World Ocean Atlas 2009, vol. 4, Nutrients (Phosphate, Nitrate, and Silicate), NOAA Atlas NESDIS, vol. 71, edited by S. Levitus, 398 pp., NOAA, Silver Spring, Md.

Gaube, P., D. B. Chelton, P. G. Strutton, and M. J. Behrenfeld (2013), Satellite observations of chlorophyll, phytoplankton biomass, and Ekman pumping in nonlinear mesoscale eddies, *J. Geophys. Res.*, *118*, 1–22, doi:10.1002/2013JC009027.

Greenwood, J., M. Feng, and A. Waite (2007), A one-dimensional simulation of biological production in two contrasting mesoscale eddies in the south eastern Indian Ocean, *Deep Sea Res. Part II*, *54*(8), 1029–1044, doi:10.1016/j.dsr2.2006.10.004.

Jia, F., L. X. Wu, J. A. Lan, and B. Qiu (2011), Interannual modulation of eddy kinetic energy in the southeast Indian Ocean by Southern Annular Mode, *J. Geophys. Res.*, *116*, C02029, doi:10.1029/2010JC006699.

José, Y., O. Aumont, E. Machu, P. Penven, C. L. Moloney, and O. Maury (2013), Influence of mesoscale eddies on biological production in the Mozambique Channel: Several contrasted examples from a coupled ocean-biogeochemistry model, *Deep Sea Res. Part II*, *100*, 79–93, doi:10.1016/j.dsr2.2013.10.018.

Kawamiya, M., and A. Oschlies (2001), Formation of a basin-scale surface chlorophyll pattern by Rossby waves, *Geophys. Res. Lett.*, *28*(21), 4139–4142.

Killworth, P. D., P. Cipollini, B. M. Uz, and J. R. Blundell (2004), Physical and biological mechanisms for planetary waves observed in satellite-derived chlorophyll, *J. Geophys. Res.*, *109*, C07002, doi:10.1029/2003JC001768.

Klein, P., and G. Lapeyre (2009), The oceanic vertical pump induced by mesoscale and submesoscale turbulence, *Annu. Rev. Mar. Sci.*, *1*, 351–375, doi:10.1146/annurev.marine.010908.163704.

Kohonen, T. (2001), *Self-Organizing Maps*, Springer, Berlin.

Kouketsu, S., H. Tomita, E. Oka, S. Hosoda, T. Kobayashi, and K. Sato (2012), The role of meso-scale eddies in mixed layer deepening and mode water formation in the western North Pacific, *J. Oceanogr.*, *68*(1), 63–77, doi:10.1007/s10872-011-0049-9.

Lapeyre, G., and P. Klein (2006), Impact of the small-scale elongated filaments on the oceanic vertical pump, *J. Mar. Res.*, *64*(6), 835–851.

Legendre, P., and L. Legendre (2012), *Numerical Ecology*, Elsevier, Oxford, U. K.

Lévy, M., and P. Klein (2004), Does the low frequency variability of mesoscale dynamics explain a part of the phytoplankton and zooplankton spectral variability?, *Proc. R. Soc. London, Ser. A*, *460*(2046), 1673–1687, doi:10.1098/rspa.2003.1219.

Lévy, M., P. Klein, and A.-M. Treguier (2001), Impact of sub-mesoscale physics on production and subduction of phytoplankton in an oligotrophic regime, *J. Mar. Res.*, *59*(4), 535–565.

Liu, Y., and R. H. Weisberg (2011), A review of self-organizing map applications in meteorology and oceanography, in *Self-Organizing Maps: Applications and Novel Algorithm Design*, edited by J. I. Mwasiagi, pp. 253–272, InTech, Rijeka, Croatia. [Available at http://www.intechopen.com/books/self-organizing-maps-applications-and-novel-algorithm-design/a-review-of-self-organizing-map-applications-in-meteorology-and-oceanography.]

Liu, Y., R. H. Weisberg, and C. N. Mooers (2006), Performance evaluation of the self-organizing map for feature extraction, *J. Geophys. Res.*, *111*, C05018, doi:10.1029/2005JC003117.

Ma, J., Y. Du, H. Zhan, H. Liu, and J. Wang (2014), Influence of oceanic Rossby waves on phytoplankton production in the southern tropical Indian Ocean, *J. Mar. Syst.*, *134*, 12–19, doi:10.1016/j.jmarsys.2014.02.003.

Mahadevan, A., L. N. Thomas, and A. Tandon (2008), Comment on " Eddy/wind interactions stimulate extraordinary mid-ocean plankton blooms," *Science*, *320*(5875), 448–448, doi:10.1126/science.1152111.

Martin, A. P., and K. J. Richards (2001), Mechanisms for vertical nutrient transport within a North Atlantic mesoscale eddy, *Deep Sea Res. Part II*, *48*(4), 757–773.

McGillicuddy, D., and A. Robinson (1997), Eddy-induced nutrient supply and new production in the Sargasso Sea, *Deep Sea Res. Part I*, *44*(8), 1427–1450.

McGillicuddy, D., A. Robinson, D. Siegel, H. Jannasch, R. Johnson, T. Dickey, J. McNeil, A. Michaels, and A. Knap (1998), Influence of meso-scale eddies on new production in the Sargasso Sea, *Nature*, *394*(6690), 263–266.

McGillicuddy, D. J., et al. (2007), Eddy/wind interactions stimulate extraordinary mid-ocean plankton blooms, *Science*, *316*(5827), 1021–1026, doi:10.1126/science.1136256.

McGillicuddy, D. J., J. R. Ledwell, and L. A. Anderson (2008), Response to Comment on "Eddy/Wind Interactions Stimulate Extraordinary Mid-Ocean Plankton Blooms," *Science*, *320*(5875), 448, doi:10.1126/science.1148974.

Moore, T. S., R. J. Matear, J. Marra, and L. Clementson (2007), Phytoplankton variability off the Western Australian Coast: Mesoscale eddies and their role in cross-shelf exchange, *Deep Sea Res. Part II*, *54*(8-10), 943–960, doi:10.1016/j.dsr2.2007.02.006.

Not, F., et al. (2008), Protistan assemblages across the Indian Ocean, with a specific emphasis on the picoeukaryotes, *Deep Sea Res. Part I*, *55*(11), 1456–1473, doi:10.1016/j.dsr.2008.06.007.

Oschlies, A., and V. Garcon (1998), Eddy-induced enhancement of primary production in a model of the North Atlantic Ocean, *Nature*, *394*(6690), 266–269.

Paterson, H. L., M. Feng, A. M. Waite, D. Gomis, L. E. Beckley, D. Holliday, and P. A. Thompson (2008), Physical and chemical signatures of a developing anticyclonic eddy in the Leeuwin Current, eastern Indian Ocean, *J. Geophys. Res.*, *113*, C07049, doi:10.1029/2007JC004707.

Pearce, A., and R. Griffiths (1991), The mesoscale structure of the Leeuwin Current: A comparison of laboratory models and satellite imagery, *J. Geophys. Res.*, *96*(C9), 16,739–16,757.

Quartly, G. D., and M. A. Srokosz (2003), A plankton guide to ocean physics: Colouring in the currents round South Africa and Madagascar, *Ocean Challenge*, *12*(3), 19–23.

Redfield, A. C. (1958), The biological control of chemical factors in the environment, *American Scientist*, *46*(3), 205–221.

Reusch, D. B., R. B. Alley, and B. C. Hewitson (2005), Relative performance of self-organizing maps and principal component analysis in pattern extraction from synthetic climatological data, *Polar Geogr.*, *29*(3), 188–212, doi:10.1080/789610199.

Richardson, A. J., C. Risien, and F. A. Shillington (2003), Using self-organizing maps to identify patterns in satellite imagery, *Prog. Oceanogr.*, *59*(2-3), 223–239, doi:10.1016/j.pocean.2003.07.006.

Sathyendranath, S., V. Stuart, A. Nair, K. Oka, T. Nakane, H. Bouman, M.-H. Forget, H. Maass, and T. Platt (2009), Carbon-to-chlorophyll ratio and growth rate of phytoplankton in the sea, *Mar. Ecol. Prog. Ser.*, *383*(7), doi:10.3354/meps07998.

Waite, A., P. Thompson, S. Pesant, M. Feng, L. Beckley, C. Domingues, D. Gaughan, C. Hanson, C. Holl, and T. Koslow (2007), The Leeuwin Current and its eddies: An introductory overview, *Deep Sea Res. Part II*, *54*(8), 789–796, doi:10.1016/j.dsr2.2006.12.008.

Warner, J. C., C. R. Sherwood, H. G. Arango, and R. P. Signell (2005), Performance of four turbulence closure models implemented using a generic length scale method, *Ocean Modell.*, *8*(1), 81–113, doi:10.1016/j.ocemod.2003.12.003.

Wong, C., F. Whitney, R. Matear, and K. Iseki (1998), Enhancement of new production in the northeast subarctic Pacific Ocean during negative North Pacific index events, *Limnol. Oceanogr.*, *43*(7), 1418–1426.